Journal of Colloid and Interface Science **255,** 177–188 (2002)
doi:10.1006/jcis.2002.8604

A Conductance Study of Reducing Volume Liquid Bridges

Thodoris D. Karapantsios* and Margaritis Kostoglou†,[1]

**Division of Chemical Technology, Department of Chemistry, Aristotle University of Thessaloniki, Univ. Box 116, 54124 Thessaloniki, Greece; and †Chemical Process Engineering Research Institute, P.O. Box 1517, 54006 Thessaloniki, Greece*

Received September 17, 2001; accepted July 15, 2002

This work demonstrates how electrical conductance measurements can be employed for the study of liquid bridge behavior when their volume varies with time while their separation distance remains constant. The liquid bridges are edge pinned between two vertical, identical rods (r-bridges) at varying separation distances. Liquid evaporation is used as a means of reducing the bridge volume in a continuous smooth fashion. A zero-order continuation sequence with respect to Bond number and liquid bridge volume is combined with the shooting method for the solution of the Young–Laplace equation to give the liquid bridge shape as a function of its instantaneous volume. A novel, very efficient computational scheme is developed based on singular perturbation expansion for the solution of the Laplace equation in the liquid bridge to compute its electrical conductance that proved faster by orders of magnitude compared to other alternative approaches. The potential for estimating the liquid bridge characteristics or the evaporation rate by matching the experimental and theoretical results is discussed extensively.

Key Words: **liquid bridge; evaporation; electrical conductance.**

INTRODUCTION

The study of liquid bridges between solid surfaces has been the subject of extensive research due to the large number of applications in which liquid bridges are encountered. Some examples are the study of the distribution of phases in porous media with respect to oil recovery applications, adsorption hysteresis in porous adsorbents, capillary evaporation/condensation, and the binder-induced agglomeration of particles which is of importance in operations such as flotation, coating, flocculation, and granulation.

In order to determine the shape of a liquid bridge, the surface tension of the liquid and its contact angle with the solid are needed. In many cases these two parameters are directly estimated from experimental evidence of liquid bridge behavior. This is actually the inverse problem, i.e., to estimate surface tension or/and contact angle from liquid bridge characteristics. One way to do this is by measuring the force exerted by the liquid bridge to its supporting solid boundaries. However, it appears that force measurements suffer from inevitable stability problems which require excessively meticulous procedures and further filtering of the data. Particularly when working with solid spheres, buoyancy corrections may make force data reduction very cumbersome (1). Errors from these sources may be appreciable considering the very small size of the bridges. Another approach is to identify the complete liquid bridge profile, using image processing techniques. In a recent work (2), the effective electrical conductance of conducting liquid bridges is suggested as a characterestic parameter from which liquid bridge features can be directly deduced. Electrical conductance was measured easily using a modified version of a technique originally developed in (3) to study flow characteristics in thin liquid films. In (2), the conductance of a constant volume liquid bridge was measured and analyzed with respect to change of bridge length. Here, the conductance technique is extended to the case of a liquid bridge with an evolving (reducing) volume. From an experimental point of view this can be easily realized by exploiting the evaporation of liquid from the bridge. Provided that the driving force for evaporation is small enough, liquid bridge temperature can be considered effectively constant.

The equilibrium shape of liquid bridges can be found from the solution of the Young–Laplace equation which has been the subject of many works. An early account is given in (4). Among the various bridge configurations, considerable attention has been given to the shape of liquid bridges between two spherical particles as a prototype for the study of phenomena (e.g., evaporation, condensation, oil recovery, etc.) in porous media. In particular, when the two spheres are in contact, then the liquid bridges are also called menisci. The menisci between contacting spheres has been studied by Melrose (5) for zero Bond number and Saez and Carbonel (6) for nonzero Bond number. The more general problem of liquid bridges between spheres has been studied by Erle *et al.* (7) (for zero contact angle), De Bisschop and Rigole (8), and Lian *et al.* (9) for zero Bond number. Recently, Simons *et al.* (10) gave approximate expressions for the attractive force imposed to the pair of spheres by the liquid bridge in the context of particle agglomeration. This force has been measured in (11).

The liquid bridges between plane surfaces have been studied by Fortes (12) for restricted (rods) and infinite (with contact angle as parameter) surfaces and for zero Bond number. The study of these liquid bridges in a gravity field was made by

[1] To whom correspondence should be addressed. Fax: +30 310 996209. E-mail: kostoglou@cperi.certh.gr.

0021-9797/02 $35.00

Boucher and Evans (13) for restricted surfaces and by Boucher *et al.* (14) for infinite surfaces. Latter, a stability analysis was given for the restricted surfaces problem and zero gravity by Boucher and Jones (15). The problem was extended for rotating liquid bridges on infinite surfaces by Hornung and Mittelman (16). The above references are only indicative and by no means exhaust the vast amount of literature devoted to the subject.

The main effort in this work is devoted to the development of a computational scheme that gives the electrical conductance of the bridge as a function of bridge volume. The present work has the following structure. First, the procedure for the computation of the liquid bridge shape is explained in detail. Then, a method for the computation of the conductance of the liquid bridge is developed based on the singular perturbation expansion technique. The description of the experimental procedures and results from some representative experiments comes next, and finally, the theoretical and experimental results are compared and discussed.

THEORY

Liquid Bridge Shape

Let R be the radius of the rods and D the distance between the rods (see Fig. 1). Then, the shape of the axisymmetric liquid bridge $Y(X)$ is given from the solution of the Young–Laplace equation (Y, X, and D are made dimensionless by division with R),

$$-\frac{\mathrm{d}^2Y}{\mathrm{d}X^2}\left(1+\left(\frac{\mathrm{d}Y}{\mathrm{d}X}\right)^2\right)^{-3/2}+\frac{1}{Y}\left(1+\left(\frac{\mathrm{d}Y}{\mathrm{d}X}\right)^2\right)^{-1/2} = H-\mathrm{Bo}X, \qquad [1]$$

where the Bond number is defined as $\mathrm{Bo}=\rho g R^2/\gamma$, where ρ and γ are the density and surface tension, respectively, of the liquid that constitutes the liquid bridge. H is the dimensionless (using γ/R) pressure in the bridge at $X=0$ and it is useful in the evaluation of the force between the rods due to the existence of the liquid bridge. In the present work, where the evaluation of the above force is not needed, H is only a dummy parameter that must be adjusted in order to satisfy the boundary conditions of Eq. [1].

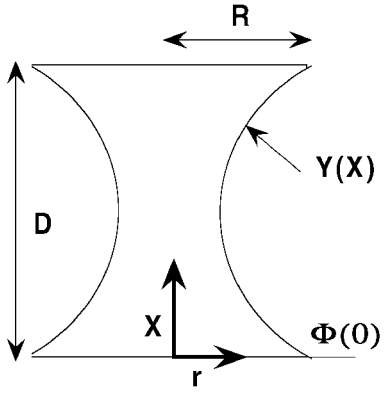

FIG. 1. Geometry of the liquid bridge.

Although in some cases the above form of the Young–Laplace equation has been solved using a finite element method (17), it is generally known that the numerical solution of this form has several problems due to pronounced sensitivity to the numerical accuracy (18). For this reason a variable transformation is suggested which results to a system of ordinary differential equations with the arc length of the liquid bridge as the independent variable,

$$\frac{\mathrm{d}\Phi}{\mathrm{d}S}=H-\mathrm{Bo}X-\frac{\sin(\Phi)}{Y} \qquad [2a]$$

$$\frac{\mathrm{d}Y}{\mathrm{d}S}=\cos(\Phi) \qquad [2b]$$

$$\frac{\mathrm{d}X}{\mathrm{d}S}=\sin(\Phi), \qquad [2c]$$

where S is the dimensionless arc length of the liquid profile from the point $(Y, 0)$ to the point (Y, X) and Φ is the angle between the profile and the horizontal. A further simplification is possible due to the fact that the total arc length of the liquid bridge is not concerned in the present work. By proper division between the equations the following simplified system with X as the independent variable arises:

$$\frac{\mathrm{d}\Phi}{\mathrm{d}X}=\frac{H-\mathrm{Bo}X}{\sin(\Phi)}-\frac{1}{Y} \qquad [3a]$$

$$\frac{\mathrm{d}Y}{\mathrm{d}X}=\frac{1}{\tan(\Phi)}. \qquad [3b]$$

The boundary conditions are $Y(0)=Y(D)=1$. The total volume of the liquid bridge (nondimensionalized with πR^3) is given as

$$V=\int_0^D Y^2(X)\,\mathrm{d}X. \qquad [4]$$

The above equation is written as a differential equation with respect to X and is added as a third equation to the system [3],

$$\frac{\mathrm{d}v}{\mathrm{d}X}=Y^2(X), \qquad [5]$$

with $v(0)=0$ and $V=v(D)$.

The system of Eqs. [3a], [3b], and [5] with the corresponding boundary conditions constitute in general a boundary value problem. From the four parameters of the problem V, D, H, and $\Phi(0)$, two must be given as input and the other two must be computed as a part of the solution of the boundary value problem.

Several strategies for the solution of the problem exist according to the selection of input variables. Using as input variables H and $\Phi(0)$, the boundary value problem is transformed to a very simpler initial one, which is directly integrated for the shape of the liquid bridge (e.g., Refs. 12 and 14). The distance D between rods can be found from the condition $Y(D) = 1$ and the liquid volume from Eq. [4], and then a table of V, D, H, and $\Phi(0)$ can be constructed for the evaluation of liquid bridge geometry.

Another approach is to use as an input variable, either H or $\Phi(0)$, and to find the other one based on the requirement that V or D must have a specific value. In this scheme also, tables such as those of the previous case can be constructed. Several aspects of this method have been used (with Newton Raphson iterations (19) or bisectional searching (9)) for liquid bridges hanging between spherical particles.

However, from an experimental standpoint it is better to have V and D as input parameters because these are the directly accessible and controlled parameters. In this case the boundary value problem has two unknowns so its solution is more difficult. This approach has been used in a closely related problem by Spencer *et al.* (20), who developed a method for the determination of interfacial tension from measurements of the force required to withdraw an axisymmetric solid body from a two-fluid interface contained in a cylindrical vessel. Their method for the solution of the problem is based on successive quadratic programming with the use of Lagrange multipliers to handle equality constraints.

In the present work a simple shooting method similar to that used in (2) is employed (the basic problem is essentially the same), but the continuation procedure is different since the main continuation parameter is now the bridge volume V and not the distance D. The problem is to solve the system [3] and [5] with the respective boundary conditions and to find the values of H and $\Phi(0)$ that give a specified liquid volume V. First, a value of H and $\Phi(0)$ is assumed and the initial value problem is integrated with the use of an explicit Runge Kutta integrator with self-adjusted step and prespecified accuracy (21) to find the $Y(D)$ and the V' value; the prime designates temporal values of the parameters. The Newton Raphson method with numerically computed derivatives is used for the correction of the H and $\Phi(0)$ values. The convergence has been achieved when $Y(D) = 1$ and $V' = V$. So, in principle, for every pair of D and V values the liquid bridge shape can be computed by the above procedure. But in practice there are additional complexities. The equations, although they are not stiff, show an excessive parametric sensitivity with respect to H. This means that the solution of Eqs. [3] and [5] can be quite different for almost identical values of H.

The existence of this parametric sensitivity means that a very good estimation of H is needed for the Newton Raphson method to converge. This problem is overcome by the use of a continuation approach. The complete procedure is as follows: For a given value of D and a given Bond number Bo, a cylindrical liquid bridge is assumed with $\mathrm{Bo}' = 0$ and $V = D$. Having an exact solution (cylindrical shape with $\Phi(0) = \pi/2$ and $H = 1$ for the zero Bond number), a zero-order continuation procedure with respect to Bo' is started. This means that the Bond number is increased and the initial values for the new Newton Raphson step is the converged values of the previous step. After the required Bond number Bo is reached, a new zero-order continuation procedure with respect to V is started from $V = D$ to the required volume value.

The above procedures are similar to the numerical integration of an initial value problem with Bo' and V as time-like variables, successively. The step size of V must be very small in order to ensure convergence of the Newton Raphson method. If values of V larger than D are to be studied, then another continuation sequence starts from $V = D$ toward the required volume value (this time by increasing V). The major advantage of the algorithm is that the entire sequence of bridge shapes and bridge conductances with respect to a reducing bridge volume for specified Bo and D is taken in just one run of the code.

The employed continuation method ensures that from the two possible solutions the stable one is always taken. This can be demonstrated using Fig. 7a of Ref. (12), which displays the possible configurations (with angle $\theta = \pi - \Phi(0)$) of liquid bridges for the present problem in V and D axes. Although that graph is for a zero Bond number, it is known that the general behavior is the same for finite Bond numbers (13). To facilitate the demonstration of the proposed procedure, the regions of the possible bridge configurations are shown qualitatively in Fig. 2. It is clear from the figure that for bridges with $\theta < \pi/2$ and V smaller than a certain value there are two possible configurations of the bridge for every V, D pair from which only that of lower θ is stable. The continuation sequence starts from the diagonal of the above-mentioned figure, first crosses the region of a unique solution, and finally passes to the region of two possible configurations. This trajectory is a straight line parallel to the V axis. The parametric sensitivity that was previously mentioned ensures that the Newton Raphson method converges to the stable solution when passing from one region to the other since it is impossible to roll toward the unstable solution that has a clearly larger θ value.

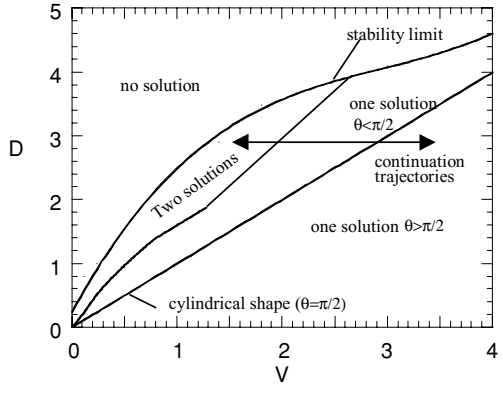

FIG. 2. Trajectories of the continuation procedure on a phase diagram of the liquid bridge.

The continuation stops when the stability limit curve is reached. At this point, rupture of the liquid bridge occurs, $V = V_{\text{rup}}$. Our code has been tested extensively to reproduce the results that are given in Fig. 7a of Ref. (12) for zero-gravity conditions.

Conductivity Problem

If an electrical potential difference exists between the two rods and the conductivity of the liquid in the bridge is uniform all over, the potential distribution in the bridge is given by the solution of the following Laplace equation:

$$\frac{1}{r}\frac{\theta}{\theta r}r\frac{\theta P}{\theta r}+\frac{\theta^2 P}{\theta X^2}=0 \qquad \text{in } 0<r<Y(X) \quad \text{and} \quad 0<X<D, \tag{6}$$

where P is the electrical potential normalized to be 1 at the one rod and 0 at the other. The boundary conditions for the above equation are

$$P=1 \qquad \text{for } X=0 \quad \text{and} \quad 0<r<1 \tag{7a}$$

$$P=0 \qquad \text{for } X=D \quad \text{and} \quad 0<r<1 \tag{7b}$$

$$\left(\frac{\theta P}{\theta \mathbf{n}}\right)_{r=Y(X)}=0, \tag{7c}$$

where $\mathbf{n}$ is the unit normal vector.

Having found the potential distribution in the bridge, the dimensionless conductance K_{app} can be computed from the relation

$$K_{\text{app}}=-2\int_0^1\left(\frac{\theta P}{\theta X}\right)_{X=0} r\,\mathrm{d}r. \tag{8}$$

The conductance is made dimensionless with σR, where σ is the specific conductivity of the liquid. The above mathematical problem is quite similar to the extensively studied problem of heat transfer in fins (22). Equation [6] can be in general solved using typical numerical methods as finite elements, finite differences, or even boundary elements. But for the present application, where for every evaporation experiment Eq. [6] must be solved many times due to the evolving computational domain shape, the above methods are computationally intractable. Some approximate solutions based on the smallness of the derivative $\mathrm{d}Y/\mathrm{d}X$ have been developed for the problem of heat transfer from fins (22). These solutions usually arise in a nonformal way but Kevorkian and Cole (23) showed that they are actually the zero-order term of a singular perturbation expansion of the solution. This zero-order term has a restricted range of validity and more terms are needed to take accurate results for realistic liquid bridge shapes. The derivation of the higher-order approximate solution which combines accuracy (at least for bridge shapes used in the present work) and computational efficiency is described next.

The X-axis is rescaled as

$$x=\frac{1}{D}X,$$

so a new parameter $\varepsilon=\frac{1}{D}$ appears. The problem can be written now as

$$\frac{\partial^2 P}{\partial r^2}+\frac{1}{r}\frac{\partial P}{\partial r}+\varepsilon^2\frac{\partial^2 P}{\partial x^2}=0 \qquad \text{in } 0<r<Y(x) \quad 0<x<1, \tag{9}$$

with boundary condition

$$\frac{\partial P}{\partial r}=\varepsilon Y'(x)\frac{\partial P}{\partial x} \qquad \text{at } r=Y(x), \tag{10}$$

and

$$P(0)=1,\ P(1)=0 \qquad \text{for } 0<r<1,$$

where prime denotes derivative with respect to x.

We will try next to solve the above problem for $\varepsilon \ll 1$. In this case the following series converges:

$$P=\sum_{i=0}^{\infty}P_i\varepsilon^{2i}, \tag{11}$$

so substituting [11] in [9] and [10], it is taken respectively,

$$\frac{\partial^2 P_i}{\partial r^2}+\frac{1}{r}\frac{\partial P_i}{\partial r}=-\frac{\partial^2 P_{i-1}}{\partial x^2}(1-\delta_{i0}) \tag{12}$$

$$\frac{\partial P_i}{\partial r}=Y'(x)\frac{\partial P_{i-1}}{\partial x}(1-\delta_{i0}) \quad r=Y(x), \tag{13}$$

where δ_{ij} is the Kronecker delta (1 for $i=j$ and 0 for $i\neq j$).

It can be inferred that the functions P_i have the following form:

$$P_i(x,r)=\sum_{j=0}^{i}B_{i,j}(x)r^{2j}. \tag{14}$$

Substituting this in [12] gives

$$\frac{1}{r}\frac{\partial}{\partial r}r\frac{\partial P_i}{\partial r}=-\sum_{j=0}^{i-1}\mathrm{B}''_{i-1,j}r^{2j}, \tag{15}$$

where the prime denotes the derivative with respect to x.

Integrating twice with respect to r results in

$$P_i=-\sum_{j=0}^{i-1}B''_{i-1,j}\frac{r^{2j+2}}{(2j+2)^2}+c_1\ln(r)+c_2, \tag{16}$$

where the integration constants c_1, c_2 are in general functions of x. The requirement that P_i must be finite at $r=0$ leads to $c_1=0$.

Now, substituting P_i from [14] to [16] and equating the terms having the same power of r yields

$$B_{i,j} = -\frac{B''_{i-1,j-1}}{(2j)^2} \qquad \text{for } i \geq 1 \quad \text{and} \quad 1 \leq j \leq i. \qquad [17]$$

The series form of P_i (Eq. [14]) is substituted at the boundary condition Eq. [13] to give

$$\sum_{j=1}^{i} 2j B_{i,j} (Y(x))^{2j-1} = Y'(x) \sum_{j=0}^{i-1} B'_{i-1,j} (Y(x))^{2j} \qquad [18]$$

Using [17] to replace $B_{i,j}$ on the left-hand side of [18] and changing the summation index leads to

$$\sum_{j=0}^{i-1} \frac{B''_{i-1,j}}{2(j+1)} (Y(x))^{2j+1} = -Y'(x) \sum_{j=0}^{i-1} B'_{i-1,j} (Y(x))^{2j}. \qquad [19]$$

Multiplying the above equation with $2Y(x)$ and using the product rule of differentiation (inversely) results in

$$\sum_{j=0}^{i-1} \frac{1}{(j+1)} \frac{\mathrm{d}}{\mathrm{d}x} (Y(x))^{2j+2} \frac{dB_{i-1,j}}{dx} = 0. \qquad [20]$$

An integration with respect to x leads to the following ordinary differential equation ($i \geq 1$):

$$\frac{\mathrm{d}B_{i-1,0}}{\mathrm{d}x} = -\frac{(1-\delta_{i-1,0})}{(Y(x))^2} \sum_{j=1}^{i-1} \frac{1}{(j+1)} (Y(x))^{2j+2} \frac{\mathrm{d}B_{i-1,j}}{\mathrm{d}x} + \frac{c}{(Y(x))^2}, \qquad [21]$$

where c is an integration constant.

All the functions $B_{i,0}$ can be determined from the solution of Eq. [21] and the functions $B_{i,j}$ with $j > 0$ from Eq. [17]. The solution of Eq. [21] requires the values of $B_{i,0}(0)$ and $B_{i,0}(1)$. Applying directly the boundary conditions at $x = 0$ and $x = 1$ for the series [14] leads to the new boundary conditions $B_{i,j}(0) = B_{i,j}(1) = 0$ for all i and j except $B_{0,0}(0) = 1$. But the system of Eqs. [17] and [21] is not capable of satisfying the above boundary condition. Solving [21] for $B_{0,0}$ and substituting it in [17] to find $B_{1,1}$ results in $B_{1,1}(0) \neq 0$. Here the singular character of the problem is revealed, that is, the regular (outer) expansion is not able to admit the boundary conditions. So, a different (inner) expansion is needed in the regions of $x = 0$ and $x = 1$, which satisfy the boundary conditions at the rods and matches the outer expansion away from them. The inner expansion and the matching procedure are too tedious to be referred to here. What is important is that they lead to a very simple result for the boundary conditions of the first two terms of the outer expansion $P_0(0, r)$, $P_0(1, r)$, $P_1(0, r)$, and $P_1(1, r)$; i.e., the cross section average of the above functions must be zero except $P_0(0, r)$, which has a cross section average equal to 1. Unfortunately, such a simple relation cannot be found for the higher order terms of the expansion.

By employing the constraints on the cross-section average, the boundary conditions for the first two terms of the outer problem take the form

$$B_{0,0}(0) = 1 \qquad [22a]$$

$$B_{0,0}(1) = 0 \qquad [22b]$$

$$B_{1,0}(0) = -\frac{1}{2} B_{1,1}(0) \qquad [22c]$$

$$B_{1,0}(1) = -\frac{1}{2} B_{1,1}(1). \qquad [22d]$$

Now, one can proceed to the solution of the outer problem for the first two terms of the series [14].

Equation [21] is integrated using [22a] as initial condition and the constant is found from the condition [22b]. The result is

$$B_{0,0}(x) = \frac{1}{L} \int_x^1 \frac{1}{(Y(x))^2} \, \mathrm{d}x,$$

where

$$L = \int_0^1 \frac{1}{(Y(x))^2} \, \mathrm{d}x. \qquad [23]$$

Substitution of the above in Eq. [17] with $i = j = 1$ yields

$$B_{1,1} = -\frac{1}{2L} \frac{Y'(x)}{(Y(x))^3} \qquad [24]$$

Employing this, Eq. [21] for $i = 2$ takes the form

$$\frac{\mathrm{d}B_{1,0}}{\mathrm{d}x} = \frac{1}{4L} \left(\frac{Y''(x)}{Y(x)} - 3 \frac{(Y'(x))^2}{(Y(x))^2} \right) + \frac{c}{(Y(x))^2}. \qquad [25]$$

This equation must be solved for $B_{1,0}(x)$ and c using the following conditions:

$$B_{1,0}(0) = -\frac{1}{2} B_{1,1}(0) = \frac{Y'(0)}{4L} \qquad [26a]$$

$$B_{1,0}(1) = -\frac{1}{2} B_{1,1}(1) = \frac{Y'(1)}{4L}. \qquad [26b]$$

The solution of [25] using as initial condition Eq. [26a] is

$$B_{1,0} = \frac{Y'(0)}{4L} + \frac{1}{4L} \int_0^x \left(\frac{Y''(x)}{Y(x)} - 3 \frac{(Y'(x))^2}{(Y(x))^2} \right) \mathrm{d}x + c \int_0^x \frac{1}{(Y(x))^2} \, \mathrm{d}x. \qquad [27a]$$

By substitution of the above in [26b], c is found to be

$$c = \frac{1}{4L^2}\left[Y'(1) - Y'(0) + \int_0^1 \left(\frac{Y''(x)}{Y(x)} - 3\frac{(Y'(x))^2}{(Y(x))^2} \right) \mathrm{d}x \right]. \quad [27b]$$

So, the second order in ε approximation of the potential distribution in the bridge has been found as

$$P(x, r) = B_{0,0}(x) + (B_{1,0}(x) + B_{1,1}(x)r^2)\varepsilon^2. \quad [28]$$

The conductance is then given as

$$K_{\text{app}} = -\frac{2}{D}\int_0^1 \left(\frac{\partial P}{\partial x}\right)_{x=0} r\,\mathrm{d}r = -\frac{1}{D}\left(B'_{0,0}(0) + \left(B'_{1,0}(0) + \frac{1}{2}B'_{1,1}(0) \right)\varepsilon^2 \right). \quad [29]$$

Using the corresponding relations for $B_{i,j}$ yields

$$K_{\text{app}} = \frac{1}{DL} - \frac{\varepsilon^2}{4DL^2}\left[Y'(1) - Y'(0) - \int_0^1 \left(\frac{Y''(x)}{Y(x)} - 3\frac{(Y'(x))^2}{(Y(x))^2} \right) \mathrm{d}x \right]. \quad [30]$$

By writing the integrand as $Y^2(\frac{Y'}{Y^3})'$ and integrating by parts, the above relation can be considerably simplified:

$$K_{\text{app}} = \frac{1}{DL} - \frac{\varepsilon^2}{2DL^2}\int_0^1 \left(\frac{Y'(x)}{Y(x)} \right)^2 \mathrm{d}x. \quad [31]$$

Finally, returning to the initial axial coordinate X the result is

$$K_{\text{app}} = I_1^{-1}\left(1 - I_2 I_1^{-1}/2\right) \quad [32a]$$

$$I_1 = \int_0^D (Y(X))^{-2}\,\mathrm{d}X \quad [32b]$$

$$I_2 = \int_0^D \left(\frac{Y'(X)}{Y(X)} \right)^2 \mathrm{d}X. \quad [32c]$$

The correction to the zero-order solution, $K_{\text{app}} = I_1^{-1}$, is proportional to the mean value of the square of the normalized surface slope along the bridge. The raise to the square has to do with the cylindrical (axisymmetric) shape of the bridge. The computation of the definite integrals I_1 and I_2 can be easily embodied to the algorithm already used to solve for the bridge shape. They are transformed to two ODEs, which by using [3b] for the computation of the derivative in [32c], take the form

$$\frac{\mathrm{d}\iota_1}{\mathrm{d}X} = \frac{1}{Y^2} \quad [33a]$$

$$\frac{\mathrm{d}\iota_2}{\mathrm{d}X} = \frac{1}{(Y\tan(\Phi))^2}, \quad [33b]$$

with $\iota_1(0) = \iota_2(0) = 0$ and $\iota_1(D) = I_1$ and $\iota_2(D) = I_2$.

Equations [33a] and [33b] are added to the system of [3a], [3b], and [5]. However, for computational economy they are switched on only after the convergence criterion for the liquid bridge shape has been fulfilled. The computational cost for the evaluation of K_{app} in this way is really insignificant and many orders of magnitude smaller than using the classical discretization methods.

EXPERIMENTAL SETUP AND PROCEDURES

The experimental set-up is similar to that of Kostoglou and Karapantsios (2) (Fig. 3), with only some modifications in the electronic circuitry. Liquid bridges are edge-pinned between the tips of two equal solid rods which are aligned vertically. The upper rod is coupled with a precision cathetometer with a resolution of 5 μm/division. The cathetometer is used to adjust the separation distance between the rods prior to measurements. Rods are constructed of bronze, an excellent electrical conductor. The free ends of the rods are carefully machined to be knife-edged circles. Electrical connection of the rods is achieved through attached lead wires. The rods used in this study have radii of 1.575, 1.495, and 0.865 mm. The respective Bond numbers for the rods are 0.36, 0.32, and 0.11.

The cathetometer with the liquid bridge is placed inside a temperature/humidity-regulated chamber. In this work, temperature is regulated to $20 \pm 1^\circ$C and relative humidity to $85 \pm 2\%$. As an extra means of checking on the relative humidity of the chamber, a glass beaker containing a saturated solution of

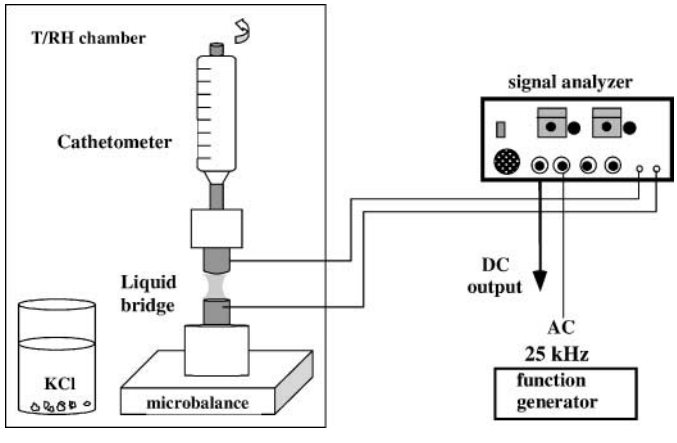

FIG. 3. Schematic diagram of the experimental setup.

potassium chloride is placed inside the chamber. To eliminate forced convective air currents around the liquid bridge, the air-circulation fan of the chamber is switched off right before the formation of the bridge. Even under such conditions the evaporation rate from the liquid bridges inside the chamber was not constant but varied in a rather narrow range. It is seen that electrical measurements can sense these small differences in the evaporation rate with a high degree of sensitivity.

An ultraprecision microsyringe is used to deposit the fluid that forms the liquid bridges. Uncertainty in withdrawing a reproducible amount of liquid from the microsyringe needle is a matter of concern, this effect being amplified on a percentage basis with smaller quantities of liquid. For the experiments performed in this study, the error in liquid volume is 1% at most determined gravimetrically by accurately weighting the liquid bridge to the fifth significant digit (10^{-5} g).

The liquid used in this work was deaerated tap water, filtered mechanically to remove suspended particles larger than 1 μm. The specific conductivity of the water at 20°C in the tests was 690 μS/cm, whereas its surface tension, determined by both the Wilhelmy slide and the ring methods, measures 65 ± 0.2 mN/m. The possible effect of the variation of these properties with temperature and bridge volume is discussed in a subsequent section.

Each experiment starts with initially setting the separation distance between the rods. Then, a liquid bridge of precisely known volume is formed. The liquid volume is selected such that it allows sufficient time before evaporation snaps the bridge**.** The initial shape of the liquid bridge is not a matter of concern since the data reduction analysis takes care of it. In all our experiments the liquid bridge is considered to remain attached to the solid rods at their circular edge. During the meniscus displacement—as a result of liquid evaporation—the apparent electrical conductance of the bridge is continuously recorded. The conductance probe comprises the two metallic rods serving as electrodes. An ac carrier voltage of 1.5 V (peak-to-peak) is applied across the probe at a frequency of 25 kHz in order to suppress undesirable electrode polarization and capacitive impedance. The response of the probe is fed to a custom-made analyzer–demodulator, similar to that employed by Karapantsios and co-workers (3). Particular attention was given to achieving a satisfactory sensitivity over an extended liquid bridge configuration in order to cope with the demands of the present study. For this, a special demodulation circuitry was included in the analyzer. This circuit acted to demodulate the peaks of the output signal synchronously using the source oscillator to create square pulses of the same frequency as the reference. A two-stage cascade phase adjustment allowed the pulses to scroll about and intersect the carrier signal at any point along the cycle (where the signal from the probe was desired to be sampled), thus converting it to an appropriate analog dc voltage signal. The user-selected amplitude of each cycle of the output was stored on a capacitor and fed to an output terminal through a buffer amplifier.

The signal from the electronic unit is monitored by a digital voltmeter, whereas the high-frequency carrier and pulse signals

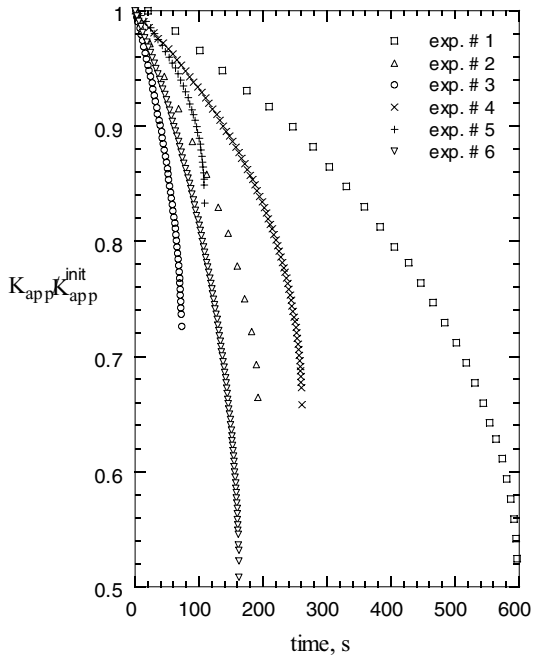

FIG. 4. Normalized apparent conductance (K_{app}/K_{app}^{init}) curves measured during the evaporation of different liquid bridges. Conditions of each experiment are presented in Table 1.

are monitored by a dual-band oscilloscope. In addition, the signal is simultaneously collected and stored in a microcomputer. Data are acquired with a variable sampling frequency in the range 1–3 Hz, which proved to be more than adequate for these experiments. The analog dc voltage output of the analyzer is converted to equivalent conductance K_{app} of the liquid between the electrodes using a calibration curve based on precision resistors. The output voltage is found to vary linearly with resistance in the entire range of resistors used. At least three records were acquired at all experimental conditions and the reproducibility was excellent. Pearson correlation coefficients among sampled curves were always above 0.99, whereas average instantaneous signal deviations were around 1%, a value close to the measured signal's noise.

Figure 4 presents recorded electrical conductance time records for different liquid bridge configurations. For clarity, only selected points at prolonged time intervals are displayed. Table 1 summarizes the conditions of the experiments in Fig. 4.

TABLE 1
Experimental Conditions of Curves Displayed in Fig. 4

Experiment	Radius (mm)	Distance (mm)	Volume (μL)
1	1.575	3.21	13.1
2	1.575	3.21	11.2
3	1.495	3.155	9.6
4	0.865	2.995	4.5
5	0.865	3.615	6.4
6	0.865	2.235	2.7

For presenting all runs in a single graph, the acquired apparent conductance values are normalized with respect to values for the initially deposited liquid bridges. Such division also eliminates errors in liquid conductivity measurements. All traces in Fig. 4 display a monotonous decay with time as expected due to the progressive elimination of water by evaporation. The decay at the beginning of all runs is more gradual since then both the water loss percentage and the change in bridge shape is small. At later times and especially at the vicinity of bridge rupture all curves are characterized by an abrupt drop of the signal. Due to the varying bridge separation distance between the runs of Fig. 4 it is not easy to directly infer the effect of liquid volume and rod radii on the conductance signal. Such arguments will be advanced in a subsequent section.

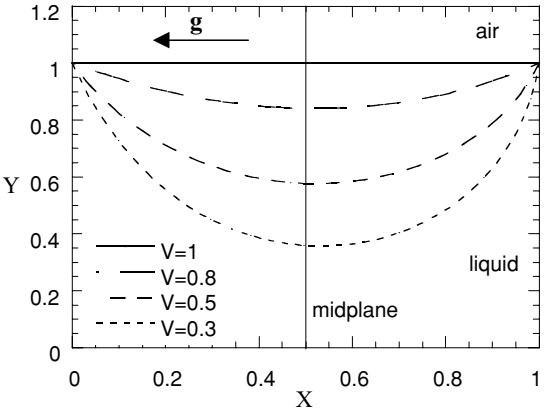

FIG. 6. Liquid bridge shape for Bo= 0.5, $D = 1$, and several dimensionless volume V values.

RESULTS AND DISCUSSION

Theoretical Results

Some theoretical results for the behavior of the liquid bridges and their electrical conductance are presented in this section. In all cases it is assumed that the solid–liquid contact angle is always smaller than $\pi - \Phi(0)$ so detachment of the bridge from the rods does not happen. The values of D that are examined in the theoretical analysis is similar to the range used in the experiments. Figure 5 shows the dimensionless rupture volume V_{rup} as a function of Bond number at several dimensionless distance values. Apparently, this volume is quite insensitive to Bond number for small values of D. For larger values of D the rupture volume is an increasing function of Bond number. As it can be seen in Fig. 5 the region of higher correlation between V_{rup} and Bo is for large D and large Bo. So, if an experimental procedure is to be developed for the evaluation of surface tension from measured rupture volumes, the experimental parameters must be selected such as D is large ($D > 3$).

Figure 6 displays the shape of liquid bridges with $D = 1$ and $\text{Bo} = 0.5$ for several V values from $V = 1$ (equivalent cylindrical shape; cylinder if under no gravity) to a volume prior to the rupture event. The bridge shape is nearly symmetrical which means that the role of gravity is insignificant in this case. Figure 7 is similar to Fig. 6, but now $D = 3$. Here the influence of gravity is obvious and the liquid bridge is quite asymmetrical with most of the liquid in the lower part of the bridge. Although the Bond number is the same for the two cases, the effect of gravity is quite different. This happens because D is actually the hydrostatic height of the bridge so the effect of gravity depends not only on Bo but on D as well. By comparing Figs. 6 and 7 it is seen that the neck radius (minimum radius of the bridge) at the rupture point is somewhat larger when the influence of gravity is significant.

Figure 8 shows the predicted variation of the apparent electrical conductance of the bridge with respect to V for several values of D and $\text{Bo} = 0$. Curves for both zero-order and first-order solutions are included (see below). As it has already been mentioned, curves of this type can be obtained by direct use of the developed code since the trajectory of decreasing V (starting from the equivalent cylindrical shape) is followed by the continuation sequence. For $\text{Bo} = 0$ the conductance of the initial cylindrical bridge is simply $1/D$. Figure 8 shows that the

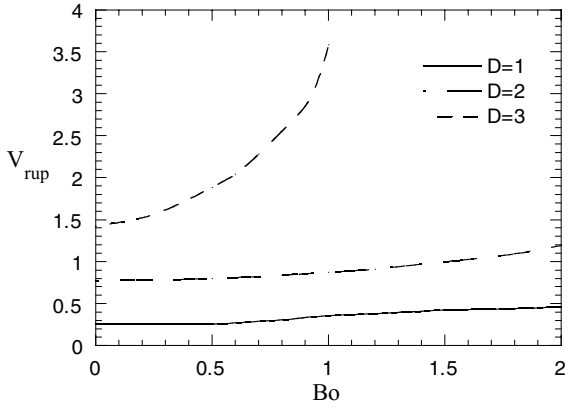

FIG. 5. Dimensionless rupture volume V_{rup} versus Bond number Bo for several values of the dimensionless distance D of the liquid bridge.

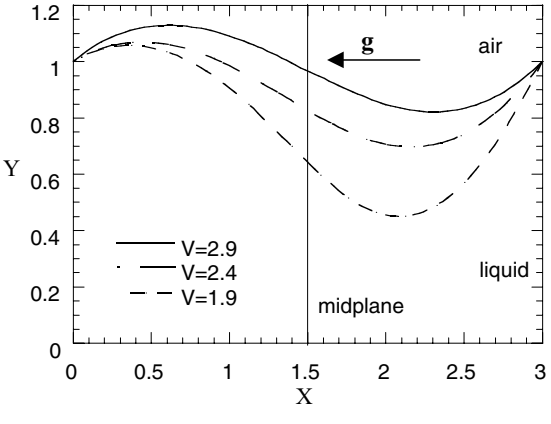

FIG. 7. Liquid bridge shape for $\text{Bo} = 0.5$, $D = 3$, and several dimensionless volume V values.

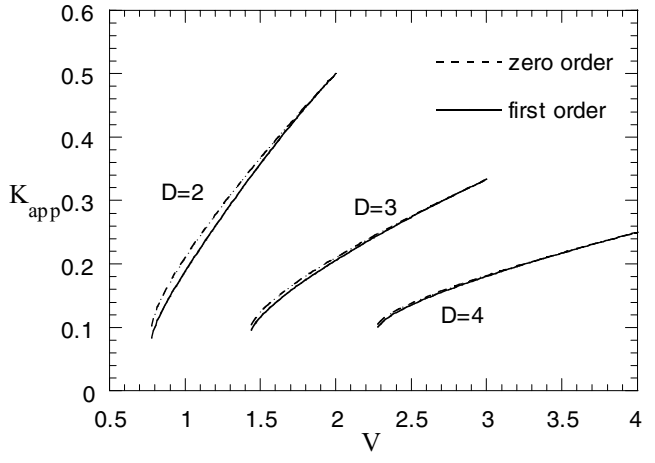

FIG. 8. Apparent conductance K_{app} versus dimensionless volume V for a liquid bridge with Bo = 0 and several D values.

conductance at the rupture point is a weakly increasing function of D. Perhaps more significant is the different slope of the curves for the different D values. The smaller the rod separation distance the higher the conductance variability with respect to volume change.

Figure 9 shows the predicted variation of the apparent conductance with volume V for $D = 2.5$ and three values of Bond number. Here it is shown more clearly than in Fig. 5 that for large Bond numbers there is a higher interrelation between Bond number and rupture distance. An important observation in both Figs. 8 and 9 is that in all cases the slope of the conductance versus V curves increases sharply prior to rupture, especially for small D values. In general, the relationship between K_{app} and V is linear for volume close to the equivalent cylindrical shape but diverges as the rupture point is approached. This divergence from linearity increases as D decreases.

In Figs. 8 and 9, the zero-order solution for K_{app} is also shown. This information is very important because from the difference

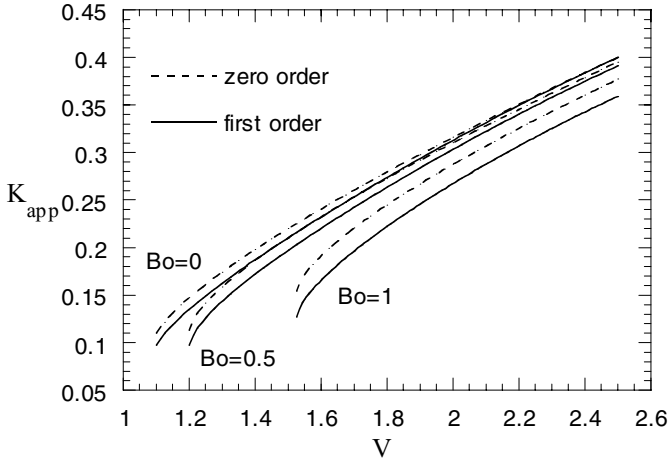

FIG. 9. Apparent conductance K_{app} versus dimensionless volume V for a liquid bridge $D = 2.5$ and several Bo values.

between the present approximation and the zero-order solution the accuracy of the approximation can be inferred. In general, the second term of the expansion of the perturbation series for K_{app} is proportional to the square of the first term, so a 10% difference between the first and zero terms means that the second term will be of order 1%; thus, the approximation is quite acceptable. In this sense, the solution developed in the present work can be safely used for $D > 1.5$, whereas for $D > 3$ (provided Bo < 0.6) even the zero-order solution is adequate. The two solutions for small Bo numbers and large V are in close proximity and diverge as V decreases. For large Bo, though, they are appreciably dissimilar, even for the equivalent cylinder volume. This is due to the fact that for large Bo (Bo ≥ 1), the bridge is highly distorted even for the equivalent cylinder volume, whereas for the other cases it has a perfectly cylindrical (Bo = 0) or a nearly cylindrical (Bo = 0.5) shape.

The *receding* contact angle between the rod material (stainless steel) and water is around 10° (24), which is smaller than the angles shown in Figs. 6 and 7. During the experiment the liquid bridge is edge-pinned to the rods and as its volume decreases the actual contact angle decreases. Had the decreasing contact angle reached the *receding* contact angle value, it would have remained at this value and then the contact line would have begun to slip on the rod. This is similar to what is shown in the work of Peppin *et al.* (25, 26), where the actual contact angle initially decreases and then remains constant as the separation distance between the supporting solids increases. Yet, in our experiments the regime of constant contact angle (slipping contact line) is never reached since the rupture of the bridge happens well above the *receding* contact angle value. So, the answer is that there is no slippage at all on the rods and this is also confirmed by optical observation.

DISCUSSION

It must be made clear that it is beyond the scope of this work to conduct an extensive experimental study of evaporation phenomena in liquid bridges. The evaporation experiments are used simply to demonstrate the merits of the technique to some potential applications and that is why we did only some representative runs for a few typical conditions.

The question that arises next is how the experimental conductance time records acquired during the volume change of the liquid bridge can be used in order to obtain information about liquid bridge characteristics. In the present case, where the bridge volume reduction is due to liquid evaporation, the fully deployed experimental curve cannot be safely used since the instantaneous evaporation rate is actually unknown. But the final measured conductance value corresponding to the rupture point does not depend on the evaporation path. It has to do only with the distance D and the Bond number. Thus, it is tempting to try to estimate the liquid surface tension, i.e., the Bond number, from the measured conductance at the rupture point. In Fig. 5, it is shown that a significant correlation between V_{rup} and Bo

exists only for large values of $D(D > 3)$ and a particular range of Bo which depends on D. In general, the conductance is a linear function of the bridge volume for constant D, so in principle a gross estimation of surface tension can be made provided that the parameters are in the appropriate range of values.

The code developed here can be used to identify this appropriate range. A criterion for this can be the value of the derivative $\frac{\partial K_{\text{app}}^{\text{rup}}}{\partial \text{Bo}}$ at constant D and Bo. This derivative shows how errors in directly determined quantities such as $K_{\text{app}}^{\text{rup}}$ (these can be experimental, i.e., finite acquisition frequency errors in measuring conductance and bridge weight, change of bridge temperature, etc., or theoretical, i.e., approximate, solution of the Laplace equation, assumption of uniform conductivity, etc.) influence indirectly estimated quantities such as Bo. For the present experiments the above derivative is smaller than 0.05, which means that they cannot be used for surface tension estimation (a typical error of 2% in $K_{\text{app}}^{\text{rup}}$ leads to an error larger than 40% in surface tension). Nevertheless, for $D > 3$ and $\text{Bo} > 0.8$, the above derivative is smaller than unity and a reasonable estimation of surface tension is possible. The appropriate selection of D is easy, but that of Bo is more elaborate because it depends on ρ and γ of the liquid (which is to be found), and by adjusting R the bridge volume is also affected. Nevertheless, this is a point that deserves more attention and exploration.

Another possibility is to use conductance measurements for the accurate estimation of the initial volume of the liquid bridge when the parameters D and Bo are known. This can be done by first using the code to construct the theoretical curve of the ratio $K_{\text{app}}/K_{\text{app}}^{\text{rup}}$ versus volume V for the specific D and Bo. Then, the experimental value of $K_{\text{app}}^{\text{init}}/K_{\text{app}}^{\text{rup}}$ ($K_{\text{app}}^{\text{init}}$ is the apparent conductance for the initial bridge volume) is calculated and with a single interpolation among the values of the theoretical curve, the initial liquid volume can be obtained. The conductance ratio is used instead of the absolute conductance in order for the procedure to be independent from conductivity measurements. The sensitivity ratio $\frac{\partial (K_{\text{app}}/K_{\text{app}}^{\text{rup}})}{\partial V}$ at constant D and Bo is in general larger than unity so a reasonable estimation of the liquid bridge volume is always possible. For instance, the difference between directly measured bridge volumes and those estimated by the above procedure is within $\pm 2\%$.

In both the above applications, the surface tension of the liquid does not correspond to the ambient temperature but to the temperature of the evaporating interface. However, this temperature can be roughly estimated from an energy balance on the surface of the liquid bridge.

A further possibility is to use the experimental curves for the estimation of the evaporation rate. The accurate computation of the liquid bridge evaporation rate is difficult. Griffin and Loyalka (27) solved the relevant problem of condensation on liquid bridges using boundary element techniques, but under simplified conditions (isothermal, steady state, pure diffusion). In practice the air currents around the liquid bridge (due to the experimental conditions) make the situation more complex. The numerical solution of the complete problem of evaporation including convection is far from trivial (28). For these reasons the accurate experimental determination of evaporation rates from liquid bridges has increased significance.

The procedure for the transformation of the conductance curves to evaporation rate curves is as follows: First, the experimental curve $K_{\text{app}}/K_{\text{app}}^{\text{init}}$ versus time is measured. Then, for the particular experimental conditions (initial volume, D, Bo) the code is used for the construction of the theoretical curve $K_{\text{app}}/K_{\text{app}}^{\text{init}}$ versus bridge volume V. At this stage the liquid bridge volume variation is known in a parametric form; i.e., $t = f_1(s)$ from the experiments and $V = f_2(s)$ from the theory, where $s = K_{\text{app}}/K_{\text{app}}^{\text{init}}$. Using multiple interpolation the evolution curve $V(t)$ can be constructed. In order to avoid a possible small amount of noise in the experimental measurements, which may cause a problem in the estimation of evaporation rates because of the differentiation of the experimental curves, it is better to fit the curve $V(t)$ with a higher degree polynomial. An eighth-order polynomial fits almost perfectly the data of the present work. This polynomial is differentiated analytically to give the evolution of the evaporation rate.

It must be mentioned that the analysis performed in this work is based on the assumption that the conductivity is constant during the evaporation experiment. This, in turn, means that the temperature of the liquid bridge and the ion concentration remains constant. As regards the temperature this is not true because the high value of the evaporation enthalpy of water results in a temperature decrease of the evaporating liquid. Heat flow by conduction begins from the bulk of the liquid to the free surface of the bridge and since the bridge has a finite heat capacity the result is an overall decrease of bridge temperature. For the present experiments the driving force for evaporation is small (due to high value of the ambient relative humidity) and a gross quantitative analysis reveals that the decrease of the mean temperature of the bridge in the experiments is smaller than 1.5°C.

As regards the ion concentration, an elementary step would be to assume that the liquid-specific conductivity is inversely proportional to the liquid bridge volume. In principle, such a step can be easily embodied to our model but this is the case only if freshly distilled water (with added salts) is used instead of tap water. However, the situation with tap water is much more complex because of its long contact time with the ambient air. In time, CO_2 is released from the water to the environment and as a result the pH of the solution increases. This leads to the precipitation of $CaCO_3$ (29). Therefore, the free ions contributing to the conductivity of the solution are reduced and counterbalance the increase of concentration due to volume reduction of the bridge. This is also confirmed by tests where we let tap water (that used in the experiments) in a shallow dish to evaporate while recording its conductivity change with time. Even for a 50% reduction in volume the change in conductivity is no more than 3%. From a thermodynamic point of view the situation in the above experiment is similar to that of liquid bridge evaporation. The main difference is in the time scale, which depends on the ratio of

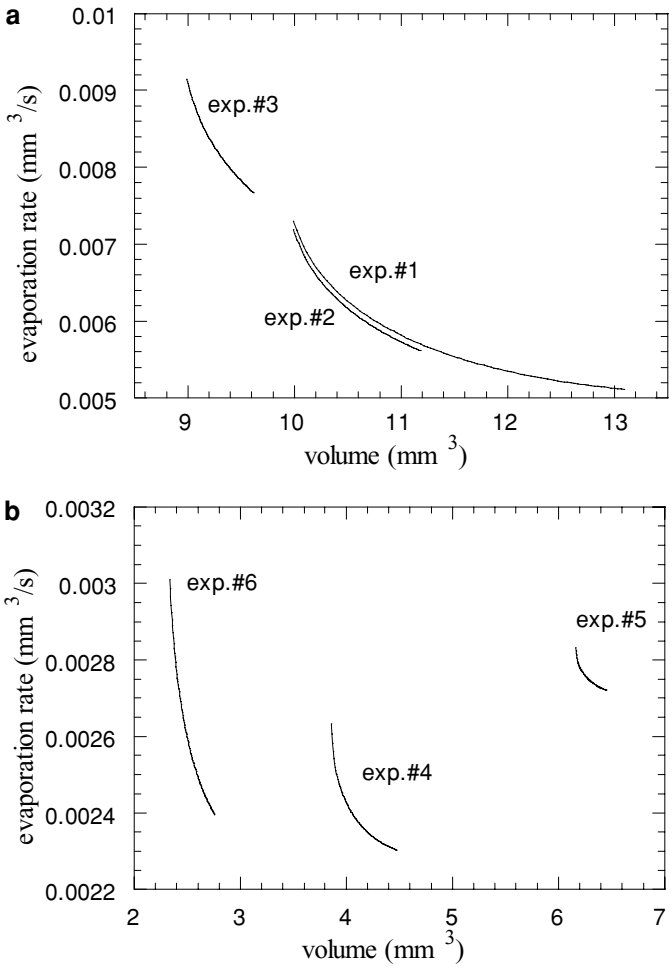

FIG. 10. Evaporation rates calculated for the liquid bridges of experiments (a) 1, 2, 3 and (b) 4, 5, 6 versus liquid bridge volume.

the evaporation area over the liquid volume. Since the rigorous modeling of the evaporation phenomena is extremely difficult to achieve, the present analysis based on the assumption of a constant liquid conductivity is an adequate approach and anyway within the required level of accuracy.

Using the above procedure the evolution of the evaporation rate for the experiments shown in Fig. 4 is computed. The computed evaporation rate is displayed versus the liquid bridge volume in Fig. 10a (experiments 1, 2, and 3) and Fig. 10b (experiments 4, 5, and 6). Evidently, the evaporation rate increases as the liquid bridge volume decreases. This behavior cannot be attributed to the change of the bridge free surface area which increases for the cases 1, 2, and 3 (but to a smaller degree than the evaporation rate) and decreases slightly for experiments 4, 5, and 6 as the liquid bridge volume decreases. So, the increase of the evaporation rate may be explained only if one assumes that the evaporation process is diffusion dominated. In this case the Laplace equation must be solved for the air outside the bridge and as it is known from the solution outside a single sphere, the evaporation rate is inversely proportional to the curvature radius (for convex surfaces). The sharp increase of the evaporation rate prior to rupture is due to the sharp decrease of the radius of curvature prior to rupture. It must be noted that whereas the transverse curvature tends to increase the evaporation rate the axial curvature has the opposite effect (concave surface). However, for bridges with large values of D the axial curvature is much smaller than the transverse one.

The increase of the evaporation rate is larger for the cases with smaller values of D. This is due to the fact that for large values of D the effect of gravity is significant and the bridge is ruptured before its radius of curvature becomes very small (cf. Figs. 6 and 7). The small difference between the evaporation rates for the experiments 1 and 2 confirms the reliability of the procedure. These two experiments differ only in the initial volume of the liquid bridge and in principle the evaporation rates should coincide. The small deviation (1.5–2.5%) between them is, at least in part, due to the smaller mean bridge temperature in experiment 1 because of the larger available time for heat transfer in the bridge. This leads to a computation of a larger evaporation rate than the real one.

One might argue that the surface tension is not constant during the evaporation experiment due to the concentration increase of impurities (surfactants) present in the tap water. The impurities in the tap water we used in our experiments decrease the surface tension from 72.75 (for ultra pure water (30)) to 65 mN/m at 20°C. In the worst case (linear regime of the Gibbs equation (31)) a reduction of 20% percent in the bridge volume (cf. Figs. 8a and 8b) and the corresponding increase of the surface concentration would lead to a surface tension of 63 mN/m. So, assuming a constant surface tension is compatible with the levels of accuracy adopted in the present work. Needless to say that a meticulous evaporation-directed study should incorporate the evolution of the liquid bridge temperature and surface tension in the model.

The success of the method presented here is based on the premise of uniform bridge conductivity. Although this assumption is valid for the present experiments with tap water (since any local concentration increase is regulated by the onset of precipitation), it does not hold for every case. For example, for water with low conductivity (with no possibility for supersaturation), the ions concentration increases as the evaporation proceeds. If the evaporation is slow enough the ions have enough time to diffuse in the bridge and the conductivity is uniform throughout the bridge (but it changes with time). This case can be handled with the tools developed in the present work by simply adding a dependence between liquid conductivity and bridge volume. On the other hand, if the evaporation is fast the ions are accumulated on the evaporation front and they do not have enough time to diffuse inward. This leads to development of conductivity profiles in the bridge. At this case the present procedure cannot be used since the diffusion equation with variable diffusivity must be solved (only a numerical solution is possible) instead of the Laplace equation.

CONCLUSIONS

In the present work an electrical conductance technique is explored as a means to study reducing volume liquid bridges. An integrated mathematical framework is developed which allows the computation of liquid bridge shape as its volume is reduced. The electrical conductance of the liquid bridge is computed through the solution of the Laplace equation in axisymmetric geometry. A novel method is proposed for the transformation of the partial differential equation in a system of two ordinary differential equations through a singular perturbation expansion. The numerical codes compute very efficiently the curves of conductance versus volume of the liquid bridge. Several experiments are performed in which the conductance of reducing volume (evaporating) bridges is measured versus time. By matching the theoretical curves with experimental time records several features of the bridge can be estimated, e.g., initial bridge volume and evolution of the evaporation rate.

REFERENCES

1. Wolfram, E., and Pinder, J., *Acta. Chem. Acad. Sci. Hung.* **100,** 433 (1979).
2. Karapantsios, T. D., and Kostoglou, M., *J. Colloid Interface Sci.* **227,** 282 (2000).
3. Karapantsios, T. D., Paras, S. V., and Karabelas, A. J., *Int. J. Multiphase Flow* **15,** 1 (1989).
4. Padday, J. F., *Pure Appl. Chem.* **48,** 485 (1976).
5. Melrose, J. C., *AIChE J.* **12,** 986 (1966).
6. Saez, A. E., and Carbonel, R. G., *J. Colloid Interface Sci.* **140,** 408 (1990).
7. Erle, M. A., Dyson, D. C., and Morrow, N. R., *AIChE J.* **17,** 115 (1971).
8. De Bisschop, F. R. E., and Rigole, W. J. L., *J. Colloid Interface Sci.* **88,** 117 (1982).
9. Lian, G., Thornton, C., and Adams, M. J., *J. Colloid Interface Sci.* **161,** 138 (1993).
10. Simons, S. J. R., Seville, J. P. K., and Adams, M. J., *Chem. Eng. Sci.* **49,** 2331 (1994).
11. Fairbrother, R. J., and Simons, S. J. R., *Particle Particulate System Characterization* **15,** 16 (1998).
12. Fortes, M. A., *J. Colloid Interface Sci.* **88,** 338 (1982).
13. Boucher, E. A., and Evans, M. J. B., *J. Colloid Interface Sci.* **75,** 409 (1980).
14. Boucher, E. A., Evans, M. J. B., and McGarry, S., *J. Colloid Interface Sci.* **89,** 154 (1982).
15. Boucher, E. A., and Jones, T. G. J., *J. Colloid Interface Sci.* **126,** 469 (1988).
16. Hornung, U., and Mittelman, H. D., *J. Colloid Interface Sci.* **146,** 219 (1991).
17. Zasadzinski, J. A. N., Sweeney, J. B., Davis, H. T., and Scriven, L. E., *J. Colloid Interface Sci.* **119,** 108 (1987).
18. Pozrikidis, C., "Introduction to Theoretical and Computational Fluid Dynamics." Oxford University Press, New York, 1997.
19. Mazzone, D. N., Tardos, G. I., and Pfeffer, R., *J. Colloid Interface Sci.* **113,** 544 (1986).
20. Spencer, J. L., Gunde, R., and Hartland, S., *Comput. Chem. Eng.* **22,** 1129 (1998).
21. Press, W. H., Teukolsky, S. A., Vetterling, W. T., and Flannery, B. P., "Numerical Recipes. The Art of Scientific Computing." Cambridge University Press, New York, 1992.
22. Michailov, M. D., and Özisik, M. N., "Unified Analysis and Solutions of Heat and Mass Diffusion." Wiley, New York, 1984.
23. Kevorkian, J., and Cole, J. D., "Multiple Scales and Singular Perturbation Methods." Springer-Verlag, New York, 1996.
24. Chandra, S., di Marzo, M., Qiao, Y. M., and Tartarini, P., *Fire Safety J.* **27,** 141 (1996).
25. Pepin, X., Rosseti, D., Iveson, S. M., and Simons, S. J. R., *J. Colloid Interface Sci.* **232,** 289 (2000).
26. Pepin, X., Rosseti, D., and Simons, S. J. R., *J. Colloid Interface Sci.* **232,** 298 (2000).
27. Griffin, J. L., and Loyalka, S. K., *J. Aerosol Sci.* **27,** 3 (1996).
28. Sirignano, W. A., "Fluid Dynamics and Transport of Droplet and Sprays." Cambridge University Press, New York, 1999.
29. Stumm, W., and Morgan, J. J., "Aquatic Chemistry: Chemical Equilibria and Rates in Natural Waters." Wiley Interscience, New York, 1996.
30. Straub, J., Rosner, N., and Grigull, U., *Wärme- und Stoffübertragung* **14,** 241 (1980).
31. White, M. L., "Clean Surfaces, Their Preparation and Characterisation for Interfacial Studies" (G. Goldfinger, Ed.). Decker, New York, 1970.